Arabian Journal for Science and Engineering (2019) 44:7465–7477
https://doi.org/10.1007/s13369-019-03783-0

RESEARCH ARTICLE - MECHANICAL ENGINEERING

Cutting Forces, Surface Roughness and Tool Wear Quality Assessment Using ANN and PSO Approach During Machining of MDN431 with TiN/AlN-Coated Cutting Tool

Pradeep V. Badiger[1] · Vijay Desai[2] · M. R. Ramesh[2] · B. K. Prajwala[3] · K. Raveendra[4]

Received: 21 August 2018 / Accepted: 14 February 2019 / Published online: 6 March 2019

Abstract
The aim of this study was to improve the life and performance of tungsten carbide turning tool inserts coated with TiN/AlN multilayer thin films using physical vapor deposition technique. Quality characteristics of the coating are evaluated using Calo and VDI 3198 tests. Thickness of the coating is found to be 3.651 μm with adhesion quality of HF1. The performance of coated tool inserts is evaluated using cutting speed (59–118 m/min), feed rate (0.062–0.125 mm/rev) and depth of cut (0.2–0.4 mm) as process parameters in turning MDN431 steel. Experimental investigation has been carried out based on full factorial design, and regression analysis was used to analyze and build the mathematical models for cutting force and surface roughness. Multi-objective optimization of the process parameters has been done with the combination of desirability approach and MOPSO technique. Optimum machining condition for least cutting force and optimum surface roughness is found to be $V_c = 59$ m/min, $f = 0.063$ mm/rev and $a_p = 0.2$ mm. Cutting force and surface roughness are reduced by 9% in TiN/AlN-coated tools compared with the uncoated tool. To improve the CoD and capability of predictive regression models, ANN modeling has been adopted. ANN trained model and mathematical regression models are used to predict the results and predict the responses, which follow the experimental data with minimum absolute error. The predicted results are validated using ANN and regression analysis found with minimum error, and developed models are adequate for further usage. Tool wear was reduced by 105% in TiN/AlN-coated tools compared with the uncoated tool.

Keywords Ti coating · Superalloy machining · PVD · PSO optimization · ANN modeling · Tool wear

List of Symbols

V_c	Cutting speed (rpm)
f	Feed rate (mm/rev)
a_p	Depth of cut (mm)
F_x	Feed force (N)
F_y	Thrust force (N)
F_z	Tangential force (N)
R_a	Surface roughness (μm)
V_b	Tool wear (μm)

✉ Pradeep V. Badiger
pvb.badiger@gmail.com

[1] Department of Mechanical Engineering, Nitte Meenakshi Institute of Technology, Bangalore 560064, India

[2] Department of Mechanical Engineering, National Institute of Technology Karnataka, Surathkal, Mangalore 575025, India

[3] Tata Consultancy Services, Bangalore 560066, India

[4] Quality Department, Oerlikon Balzers Coating India Pvt. Ltd., Bangalore 560099, India

1 Introduction

In the industrial manufacturing sector for better productivity and reducing the capital investment, any manufacturing process needs to be optimized and standardized. Among manufacturing processes, turning has been reported as a flexible machining process. All the manufacturing processes need to be optimized, and optimization techniques are used to improve the machining process by proper selection of cutting parameters. Machinability characteristics considered for the improvisation are tool wear, machined surface texture, surface roughness characteristics and cutting forces [1–9]. Incoloy, Inconel and other superalloys are hard-to-machine materials which require proper selection of cutting tool combination. Thin-film coatings on cutting tools developed using physical and chemical vapor deposition provide solutions to machining of the hard-to-machine materials [10–14]. Machinability characteristics were used to evaluate the performance of coated tools [1,6,7,15–18]. Optimization of

machinability characteristics provides a correlation between process parameters and responses [19–22]. Optimization techniques include statistical and parametric approach which provide validation and error analysis of the machinability characteristics [23–27]. Some of the researches related to machining, optimization, modeling, tool wear and coated tool performance are briefed.

Optimization techniques have been adopted to various studies which include tribological behavior of Mg composites reinforced with TiC and MoS_2 particles [28,29]. Addition of TiC and MoS_2 particles reduced coefficient of friction in Mg hybrid composites during tribological studies [28–31].

W. Grzesik et al. explained tool wear measurements during machining of Inconel 718. TiAlN/AlTiN coatings were developed on cutting tools, and performance of the coatings is evaluated using tool wear results. Abrasive wear and built-up edge are experienced during the machining [1]. K. Aslantas et al. studied tool wear of Al_2O_3–TiCN-coated insert during machining of AISI 52100. Crater wear type was dominant in both coated and uncoated tools; coated tool is more inclined toward built-up edge, whereas crater is formed using uncoated transformed into chipping [32].

M. Hanief et al. combined regression and ANN modeling for the experimentation and validation of cutting forces during machining of red brass. ANOVA was capable of predicting the results, but ANN model was found to be more accurate than regression model [4]. J. Ciurana et al. used artificial neural network (ANN) and multi-objective particle swarm optimization (PSO) for optimization and modeling of process parameters during micromachining hardened AISI H13 steel. Results indicate that proposed ANN and PSO techniques were efficient for optimization and prediction of results [33]. B. Rajesh Kumar et al. explained the response surface methodology (RSM) combined with a neural network for the modeling and prediction of rock properties during drilling [34].

R.T. Coelho et al. explained TiAlN nanocoating performed better in terms of tool wear and surface roughness during turning of hardened AISI 4340 steel among TiAlN, TiAlN nanocoating and AlCrN. TiAlN nanocoating is outperformed due to its high hardness and oxidation at high temperature [17].

Based on the literature survey, it has been found that performance of Al- and Ti-based multilayer coatings on WC inserts for machinability studies is minimal. In spite of substantial growth, the optimization of machinability parameters and the influence of multilayer thin-film coating on cutting forces and surface roughness study were not fully understood. Hence, in the present work, Al and Ti multilayer coatings are developed on WC tool insert with the chemical composition of TiN/AlN. Performance of multilayer coated insert is studied based on machinability properties of MDN431 alloyed steel (widely used in turbine forgings) in comparison with the uncoated tool and the effect of machining parameters on cutting forces (F_x, F_y and F_z) and surface roughness (R_a) during the machining of MDN431 steel. Quadratic mathematical models using regression analysis and artificial neural network predictive models are developed. Adequacy of the mathematical model was determined by coefficient of determination (R^2). Machining parameters are optimized using the desirability and PSO techniques. Tool wear mechanism is studied for coated tool in comparison with the uncoated tool.

2 Experimental Work

An experimental investigation was carried out on alloyed steel MDN431 specimens of dimension 250 mm length and 30 mm in diameter. Table 1 presents the chemical composition of the test specimen. Based on operability of the cutting tool and machine tool, the pilot runs are carried out to select the machining parameters and are represented in Table 2.

Self-centered three-jaw panther lathe machine tool was used for experimental work. Kennametal Germany-make SNMG120408 WC tool insert was attached to the DSSNR2020K12 tool holder. Ti multilayer coatings were developed using PVD technique with the composition of TiN/AlN (commercially called as FTR coating) at Oerlikon Balzers Coating India Pvt., Ltd. VDI 3198 and Calo test were carried out for qualitative analysis of coating adhesion at Oerlikon Balzers Coating India Pvt., Ltd. Calo test (Anton Paar, Switzerland) is a spherical abrasion test method. To this end, a small crater is ground into a coating with a ball of known geometry, providing a tapered cross section of the film when viewed under an optical microscope. Calo test was used to measure the thickness of the thin-film coating. Coated surface was cleaned with IPA solution. Steel ball is run against the surface at 200 rpm for the period of 120–180 s in the presence of diamond paste as lubricant. Wear scar created on

Table 1 Composition of MDN431

Type of substrate	C	Mn	Si	Cr	Ni	Fe
MDN 431	0.15	0.7	0.7	17	2.5	Balance

Table 2 Experimental conditions

Levels	Speed (V_c) (m/min)	Feed rate (f) (mm/rev)	DoC (a_p) (Mm)
Level 1	59	0.062	0.2
Level 2	75	0.093	0.3
Level 3	118	0.125	0.4

the surface after the Calo test is analyzed using microscope, and coating thickness is calculated with its built-in software.

VDI 3198 test was used to measure the qualitative analysis of adhesion of coatings. Using a Brinell hardness machine (ball indenter) with the load of 100 kg for the constant dwell time, indentation is created. Deformed coatings after indentation are cross-referred with the standard to obtain the conclusion of results [35].

Mechanical properties of the coatings are evaluated using nanoindentation technique and are presented in Table 5. During the nanoindentation, a Berkovich indenter was used. Nanoindenter (Agilent G200, USA) hardness tests are conducted as per ISO 14577(1-4). At clean room conditions, all the experiments are done with loading and unloading cycles keeping depth of penetration constant (70% coating thickness). Cutting forces are measured using Kistler 9257B piezoelectric dynamometer mounted on the tool post with the help of Kistler Dynoware software 2825D-02 data acquisition system. Kistler Dynamometer 9257B is used to measure the cutting forces during the machining studies. Kistler Dynamometer 9257B is equipped with 5070A charge amplifier, which is connected to a computer with A2D Board and is controlled by Kistler 2825 DYNOWARE software. Machined surface was measured by "Mitutoyo Talysurf SJ301" surface tester, and average surface roughness (R_a) was considered; there are many different roughness parameters in use, but R_a the arithmetic mean roughness is by far the most common. Other common parameters include: R_z ten-point mean roughness and R_t the maximum height of the surface profile measured according to Standard ISO 468:1982. Five measurements were taken for R_a of each machined sample with a cutoff length (λ) of 4 mm, and average was taken as actual values. Olympus LEXT 4000, Japan-make confocal microscopy, was used to build the profile of the machined surface topography, tool wear measurement, indented surface and fretting worn surface. It uses a monochromatic laser to build the 3D profile of a surface, using which height, width and depth of the worn surfaces were measured and analyzed. Experimental results of cutting forces and surface roughness are presented in Table 6. Experiments for each combination are repeated thrice to minimize the errors and to ensure the accurate readings. Using ANN and regression analysis, predictive models for cutting force and surface roughness are developed.

2.1 Regression Analysis

In the present investigation, the full factorial design was used for the design and analysis of experiments. Based on L_{27} full factorial design, different levels of experiments are conducted for the input variables such as speed, feed rate and depth of cut, and results are mentioned in Table 6.

In regression analysis, the correlation between input parameters and output responses is established using quadratic mathematical regression model. Results are predicted for the 27 experimental combinations using the mathematical regression model. In Fig. 8, the predicted results are compared with experimental results. It was found that the predicted data by the regression model closely follow the experimental data. Multi-objective optimization for the output responses is carried out using desirability approach for minimization function (smaller is better). Desirability approach was first introduced by Suich and Deringer in 1980. The desirability approach finds experimental conditions "*targeted*" as the most advisable response value.

2.2 Multi-objective Particle Swarm Optimization

MOPSO and desirability approach are employed to achieve the optimal process parameters. MOPSO was implemented using MATLAB software, and Minitab software tool was used for desirability approach. Figures 1 and 2 represents the optimization plots for desirability and MOPSO approach respectively. The parameters of MOPSO algorithms are represented in Table 3, and the working conditions for the MOPSO model are illustrated in the algorithm. Parameters indicated in the table play a vital role in obtaining finer convergence characteristics. If the population of parti-

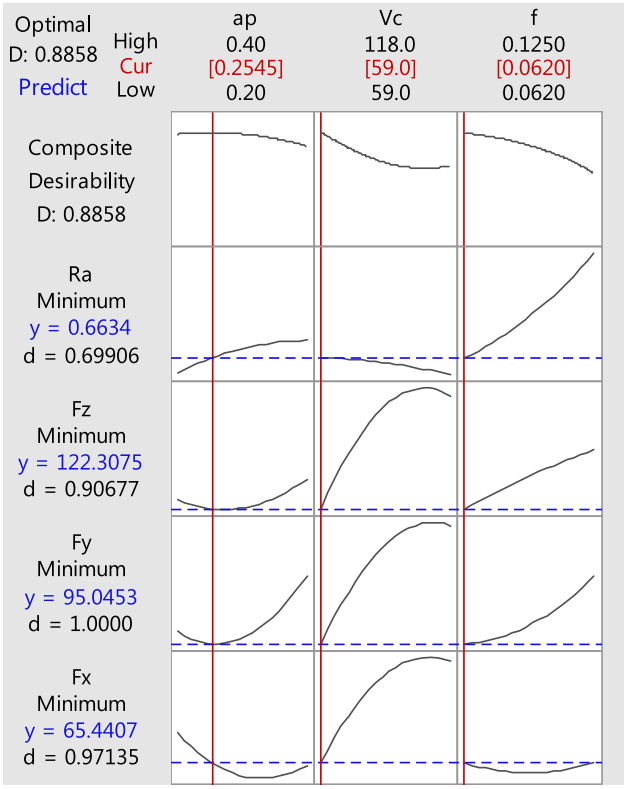

Fig. 1 Multi-objective optimization result using desirability approach

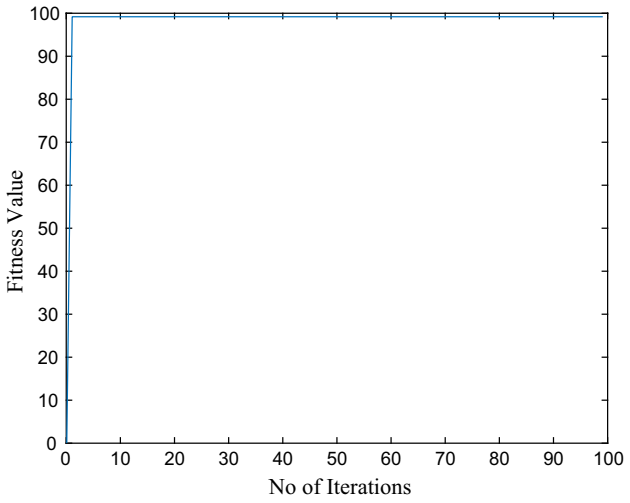

Fig. 2 MOPSO convergence plot

cle increases, the learning rate increases. In turn, the number of iterations increases in the search space. If the convergence was attained within a smaller number of iterations, then the outcome probability of getting global optimum solutions is at a higher rate. Velocity of the particles is kept within the boundary range of variables. The particles movements are governed by the mathematical functions (1, 2).

$$x_i^{t+1} = x_i^t + v_i^t. \tag{1}$$

$$v_i^t = v_i^{t-1} + c_1 r_1 (pbest^t - x_i^{t-1}) + c_2 r_2 (gbest^t - x_i^{t-1}) \tag{2}$$

where x_i^t and x_i^{t+1} are the position of the particle i in steps t and $t+1$, v_i^t is the velocity of the particle i in time t, x_i^{t-1} and v_i^{t-1} are the position and velocity in the $(t-1)$ time, c_1 and c_2 are the acceleration factors, r_1 and r_2 are the randomized vectors for the particle direction and *pbest* is the local best solution of the particle i in time t and *gbest* is the global best solution among all the particles i.

Steps involved in MOPSO algorithm

1. Initialize the population of particles (n) randomly.
2. For every particle, the fitness value (f) is evaluated.
3. If the calculated fitness value of the particle is better than the best fitness value (*pbest*) in history, then the present value is assigned as a new best fitness value (new *pbest*).
4. Choose the particle with the best fitness value among all the pbest values which are considered to be the global best (*gbest*).
5. The velocity (v_i^t) and position (x_i^t) of each particle are calculated.
6. Each particle velocity is stored to a maximum velocity. If the sum of the acceleration causes the velocity on that dimension to surpass the specified range set by the user, then velocity needs to be limited.
7. Terminate if a minimum error condition is reached or the maximum iteration is reached; else go to step 2.

Table 3 Parameters of MOPSO

Number of parameters (m)	3
Number of iterations (i)	1000
Number of particles (n)	100
Acceleration factor c_1	2
Acceleration factor c_2	2
Lower bounds of variables (LB)	[59 0.062 0.2]
Upper bounds of variables (UB)	[118 0.125 0.4]

A mathematical regression model of the output response was used as the function of the input parameters. Each output response (cutting forces and surface roughness) was considered as a objective function with a suitable weight (contribution). The objective function was used to predict the fitness value in the algorithm. A best particle with least fitness value is considered as the optimum result and optimum machining condition for multi-objectives. Optimum machining condition was used for tool wear measurement. Tool wear measurement was carried out with an increment of the constant time interval.

2.3 Artificial Neural Network Modeling

ANN modeling consists of the three steps, i.e., training, testing and validation. ANN modeling was developed according to the training parameters mentioned in Table 4.

2.3.1 ANN Training

The ANN training for the combinations of 27 FFD experiments has been carried out using "*trainglm*" learning rate training procedure of MATLAB neural network toolbox (MathWorks Incorporation 2015). The number of neurons in the hidden layer and the learning parameters are selected by a trial-and-error procedure and repeated training simulation as shown in Fig. 3.

Table 4 ANN training parameters

Learning rate (α)	0.10
Learning rate increment	10
Momentum constant (β)	0.90
Maximum number of epochs	1000

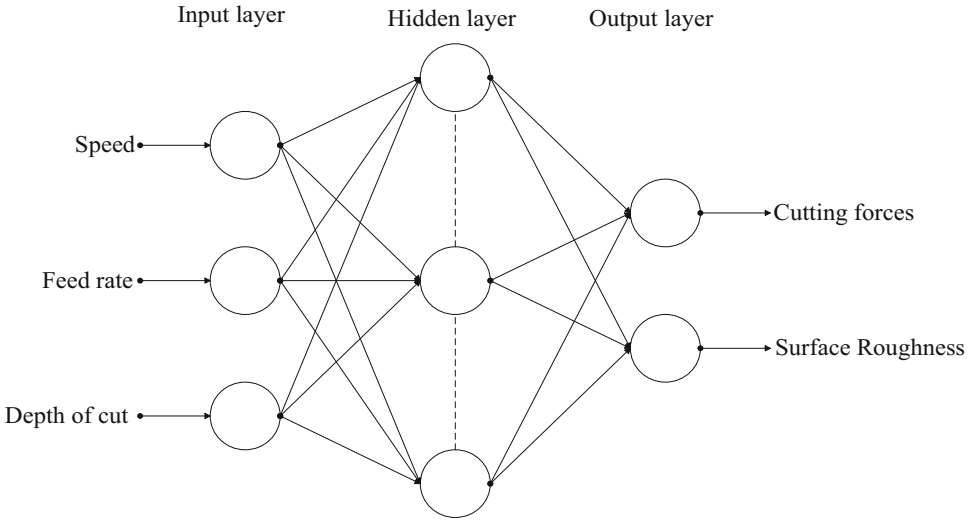

Fig. 3 Architecture of ANN network

2.3.2 ANN Testing and Validation

The trained ANN network was used to predict the results for error and accuracy by presenting 27 input process parameter combinations. For every input training combination, the predicted results of cutting forces and surface roughness are compared with corresponding experimental results. It was found that the predicted data by the ANN model closely follow the experimental data.

3 Results and Discussion

3.1 Coating Quality Characteristics

Results of Calo test and VDI 3198 tests are shown in Fig. 4. Multilayer coating was developed on the insert with the combinations of TiN and AlN layers in the sequence of TiN/AlN. The coating thickness of 3.651 µm and HF1 failure which is industrially acceptable were observed during adhesion test mentioned in Fig. 4a, b. Performance of Ti coatings is better in terms of frictional properties due to the presence of DLC, TiC and TiN phase in the coatings [36].

Mechanical properties of the thin films are investigated using nanoindentation technique, which are represented in Table 5. Hardness of the coatings was found to be 27.62 GPa and elastic modulus 490.3 GPa [37].

3.2 Machinability Studies

In the present work, machinability characteristics for MDN431 were studied using the TiN/AlN multilayer coated tool. Machinability study is carried out based on full factorial with three factors varied to three levels. Experimental results of TiN/AlN multilayer coated tools are presented in Table 6. Full factorial design has been used to develop second-order regression models represented in Eqs. (3–6), and the same is used to predict results for cutting force (F_x, F_y and F_z) and surface roughness (R_a).

Regression models developed from full factorial design:

$$F_x = \begin{pmatrix} 130 - 1287 \times a_p + 4.52 \times V_c - 2183 \times f + 2.05 \\ \times a_p \times V_c + 1856 \times a_p \times f + 10.05 \times V_c \times f \\ + 1593 \times a_p^2 - 0.0262 \times V_c^2 + 6035 \times f^2 \end{pmatrix} \quad (3)$$

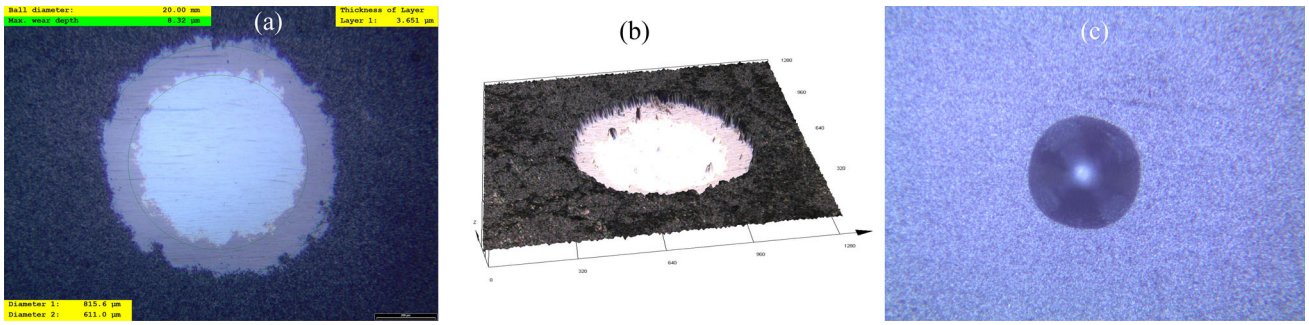

Fig. 4 **a**, **b** Calo result, **c** VDI 3198 result of FTR-coated WC–Co tool

Table 5 Mechanical properties of coatings

Coating	Hardness (GPa)	Elastic modulus (GPa)	Thickness (μm)	Surface roughness (μm)	CoF
TiN/AlN	27.62	490.3	3.651	0.52	0.35

Table 6 Taguchi FFD experimental design with results

Process parameters			TiN/AlN-coated tool			
a_p	V_c	f	F_x	F_y	F_z	R_a
0.2	59	0.062	76.76	102.2	179.3	0.54
		0.093	74.34	126.5	154.3	0.76
		0.125	76.48	136.5	175	1.05
	75	0.062	99.37	121.2	102.3	0.64
		0.093	121.6	149.2	195	0.75
		0.125	118.3	176.9	241	0.99
	118	0.062	142	180.2	242.3	0.44
		0.093	167.4	178.4	275.3	0.79
		0.125	160.2	221.9	299.8	1.05
0.3	59	0.062	60.67	100.5	127.9	0.67
		0.093	62.19	111	142	0.79
		0.125	74.77	127.4	159.6	1.05
	75	0.062	93.93	122.3	181.8	0.94
		0.093	104.5	134.8	206.9	0.83
		0.125	111.5	158.3	239.5	1.05
	118	0.062	123.8	142.9	192.1	0.65
		0.093	128.4	171.1	263.1	0.84
		0.125	146.2	196.3	280.1	0.96
0.4	59	0.062	60.36	114.5	116.4	0.77
		0.093	64.76	125.2	158.8	0.87
		0.125	74.83	144.2	190.4	1.19
	75	0.062	120.1	188.3	232	0.58
		0.093	105.8	146	237.1	0.83
		0.125	118.5	183.4	265.2	1.10
	118	0.062	144.6	166.4	191.6	0.67
		0.093	135.6	179.6	254.2	0.89
		0.125	237.7	200.6	316.9	1.15

$$F_y = \begin{pmatrix} -29.8 - 661 \times a_p + 5.38 \times V_c - 625 \times f - 2.02 \\ \times a_p \times V_c + 1914 \times a_p \times f + 3.83 \times V_c \times f \\ + 1733 \times a_p^2 - 0.02316 \times V_c^2 + 7590 \times f^2 \end{pmatrix} \quad (4)$$

$$F_z = \begin{pmatrix} -178 - 657 \times a_p + 8.33 \times V_c - 164 \times f - 2.28 \\ \times a_p \times V_c + 1077 \times a_p \times f + 13.04 \times V_c \times f \\ + 1338 \times a_p^2 - 0.0404 \times V_c^2 + 2786 \times f^2 \end{pmatrix} \quad (5)$$

$$R_a = \begin{pmatrix} 0.194 + 2.37 \times a_p + 0.002 \times V_c - 1.82 \times f \\ + 0.00092 \times a_p \times V_c - 1.65 \times a_p \times f + 0.0170 \\ \times V_c \times f - 2.87 \times a_p^2 - 0.000014 \times V_c^2 + 39.5 \times f^2 \end{pmatrix} \quad (6)$$

Regression models are represented in Eqs. (3), (4) and (5) for cutting forces F_x, F_y and F_z and Eq. (6) for surface roughness (R_a). ANOVA results for cutting forces (F_x, F_y and F_z) and surface roughness (R_a) are summarized in Table 7. The probability value (p value) is the level of marginal significance within a statistical hypothesis test representing the probability of the occurrence of a given event. The p value is used as an alternative to rejection points to provide the smallest level of significance at which the null hypothesis would be rejected. In the majority of analyses, an alpha of 0.05 is used as the cutoff for significance. If the p value is less than 0.05, we reject the null hypothesis that there is no difference between the means and conclude that a significant difference does exist. ANOVA table represents $p = 0$ for cutting forces and surface roughness, which confirms the developed regression models are significant. Coefficient of determination (R^2) gives the capability of the developed regression model. Coefficient of determination (R^2) for F_x, F_y, F_z and R_a is close to 1, which confirms developed models are adequate for the prediction of results.

3.3 Analysis of Surface Roughness

Figure 5 represents the interaction effects of surface roughness TiN/AlN multilayer coated tool. Figure 5a represents the effect of depth of cut and speed on surface roughness with a constant feed rate of 0.093 mm/rev. Figure 5b represents the

Table 7 ANOVA result summary of FTR-coated tool for FFD

Response	Sum of squares		Degrees of freedom		Mean square		F ratio	p*	CoD (R^2)
	Regression	Residual	Regression	Residual	Regression	Residual			
F_x	38,102.1	4698.8	9	17	4233.6	274.6	15.41	0.00	0.8902
F_y	25,418.5	2328.8	9	17	2824.28	136.99	20.61	0.00	0.9161
F_z	70,670.7	14,048.5	9	17	7852.3	826.38	9.46	0.00	0.8342
R_a	0.8380	0.1455	9	17	0.0931	0.0086	10.825	0.00	0.8520

*Significant at 95% confidence level

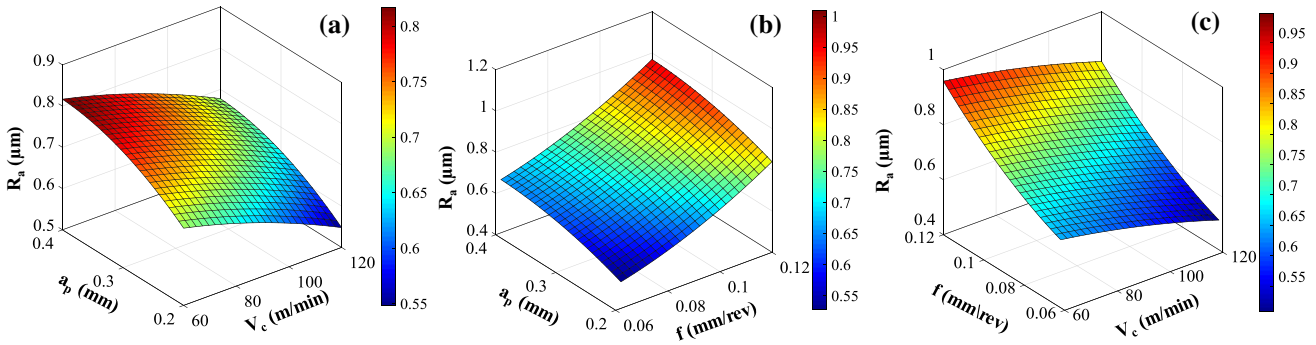

Fig. 5 Interaction plots for surface roughness during full factorial analysis

effect of depth of cut and feed rate on surface roughness with a constant speed of 75m/min. Figure 5c represents the effect of feed rate and speed on surface roughness with a constant depth of cut of 0.3 mm. The effect of feed rate and speed is phenomenal in the study of surface roughness. An increase in surface roughness is observed with an increase in feed rate. Surface roughness has been less affected by the change in depth of cut during machining. Surface roughness tends to decrease with an increase in speed.

A slight change in feed rate and speed leads to variations in the surface roughness. Contact between tool and material reduces with an increase in the speed, which leads to the reduction in the surface roughness.

Figure 6a represents the machined surface topography at the test condition of $V_c = 75$ m/min, $a_p = 0.3$ mm and $f = 0.062$ mm/rev, the surface roughness of 0.93 µm for TiN/AlN-coated tool, and the lower the feed rate, the lesser the surface roughness. Similarly, with a higher feed rate of $f = 0.125$ mm/rev represented in Fig. 6b surface roughness increased to 1.05 µm for TiN/AlN-coated tool, respectively.

Variations in feed rate and speed lead to a change in the surface roughness. With the increase in the speed, contact between tool and material reduces, which results in lesser surface roughness. With the increase in the feed rate, tool traverse speed against the work material increases, which leads to an increase in friction between tool and workpiece results in higher surface roughness [38]. With the higher cutting speed, there will more rotational torque in the material which will reduce the surface roughness [39]. Surface roughness has been reduced by 9% compared with uncoated tool. TiN/AlN coating exhibited lower magnitude of cutting force compared with uncoated tool. The lower surface roughness obtained with the coated inserts is partly attributed to the presence of hard TiN and AlN phases present in the coatings and partly due to lower coefficient of friction 0.35 [30,31].

3.4 Analysis of Cutting Force

Figure 7a–c, d–f, d–i shows the interaction effects of cutting force for F_x, F_y and F_z, respectively. Figure 7a, d, g represents the effect of depth of cut and speed on cutting forces with a constant feed rate of 0.093 mm/rev. With the increase in speed, cutting forces are increasing linearly. Figure 7b, e, h represents the effect of depth of cut and feed rate on cutting forces with a constant speed of 75m/min. With the increase in feed rate, cutting forces are increased linearly. Figure 7c, f, i represents the effect of feed rate and speed on cutting forces with a constant depth of cut 0.4 mm. With the increase in feed rate, cutting forces are increasing linearly, and with an increase in depth of cut, the cutting forces are not affected [4].

Feed rate and speed are observed linearly affecting the cutting force. For lower feed rate and speed, cutting force has been reduced, and with an increase in feed rate and speed, steady rise in the cutting force is observed. The depth of cut is not much influencing the cutting forces during machining. Speed and feed rate are contributing more (affecting the cutting force) in the factorial analysis results compared with speed [38,39]. Summary of ANOVA given in Table 7 indicated that both the regression models developed for cutting forces and surface roughness are significant ($p < 0.05$) [40].

Figure 6c represents the machined surface topography at the test condition of $V_c = 75$ m/min, $a_p = 0.2$ mm and $f = 0.093$ mm/rev, cutting forces and surface of $F_x = 121.6$ N, $F_y = 149.2$ N, $F_z = 195$ N, $R_a = 0.75$ µm observed for TiN/AlN-coated tool, respectively; the lower the depth of cut, the lesser the cutting force and surface roughness. Similarly, with a higher feed rate of $f = 0.4$ mm represented in Fig. 6d, cutting forces and surface roughness increased to $F_x = 105.8$ N, $F_y = 146$ N, $F_z = 237.1$ N, $R_a = 0.83$ µm for TiN/AlN-coated tool.

Contact between the tool and material increases with less time which leads to an increase in cutting forces. With the reduced time, the amount of materials removed increases

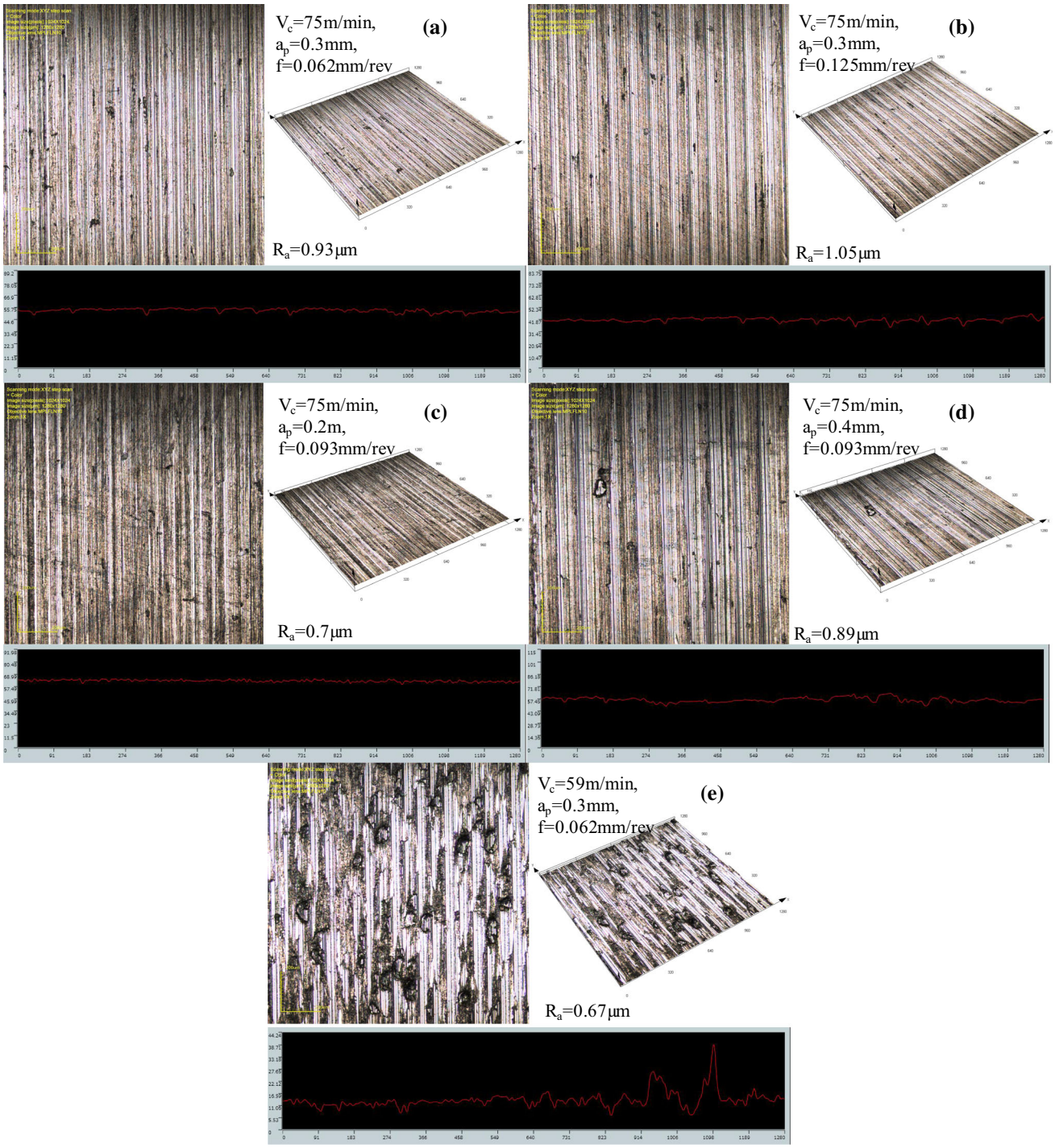

Fig. 6 Machined surface topography

which require more force to deform the material plastically and hence the increase in cutting force is observed. Tool traverse speed against the work material increases with the feed rate, and this attributes to an increase in the amount of materials removed in less time resulting in a rise in cutting force [39].

Cutting forces are reduced by 9% in compared to uncoated tool, which is due to increased hardness of coating, presence of hard nitride phases of Ti and Al nitrides. Increased hardness requires less force to deform the material plastically, which in turn resulted in lower cutting force during machining using coated inserts [28,29].

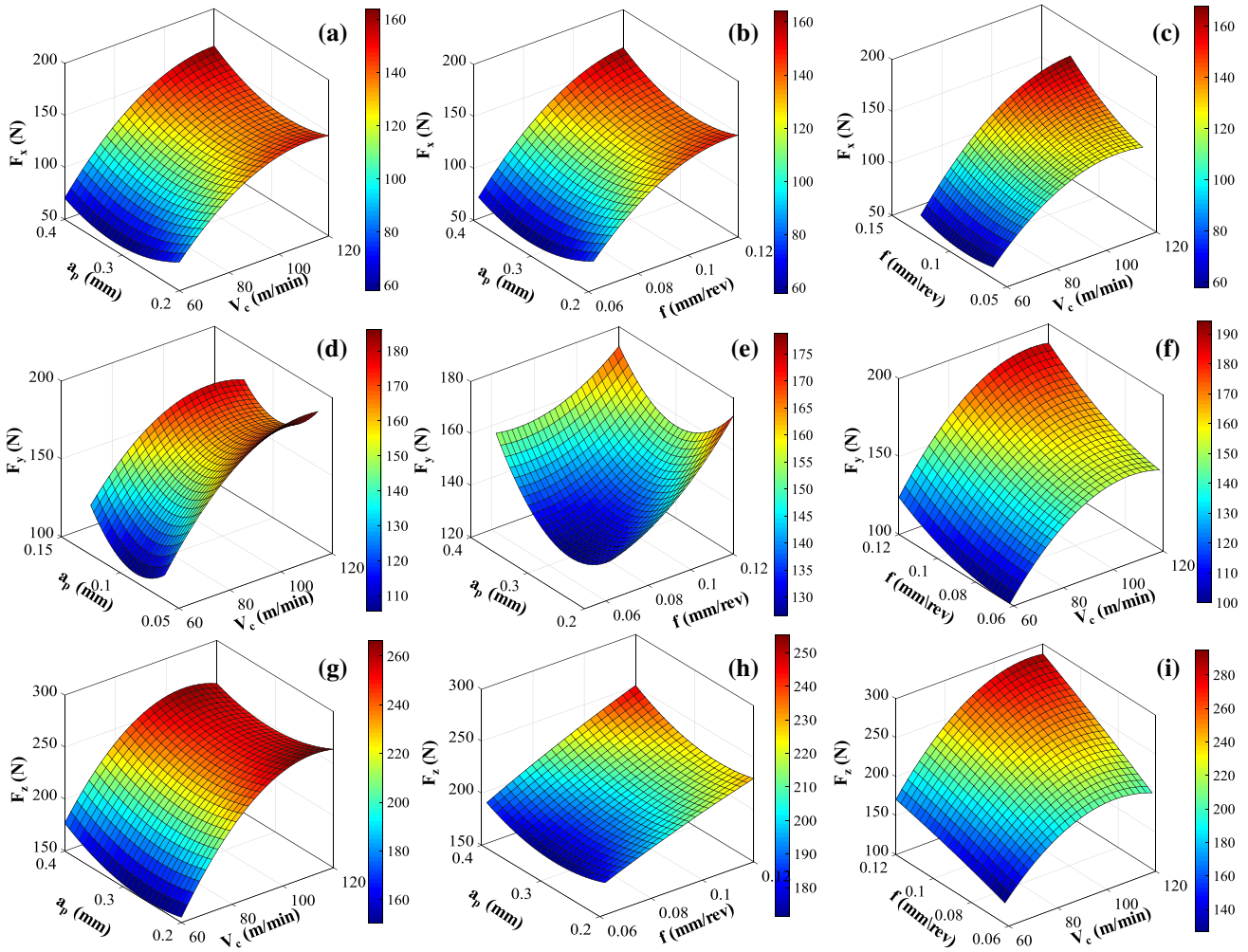

Fig. 7 Interaction plots for cutting force, **a–c** F_x, **d–f** F_y and **g–i** F_z during full factorial analysis

3.5 Optimization of the Results

Multi-objective optimization of cutting force and surface roughness is carried out using desirability and PSO optimization techniques.

Desirability approach and PSO technique for the minimization of the cutting force and surface roughness have been adopted in the present work indicated in Table 8 for the TiN/AlN multilayer coated tool.

Combination of V_c—59 m/min, f—0.062 mm/rev and a_p—0.25 mm is the optimum conditions for the machining of MDN431 using TiN/AlN multilayer coated tool obtained from both the desirability and PSO approach as given in Table 8. Machined surface topography for TiN/AlN multilayer coated tool is represented in Fig. 6e.

The depth of cut is kept at 0.3 mm, and the amount of materials deformed is optimal which in turn gives the better surface roughness and lower cutting forces. The feed rate of 0.062 mm/rev is ideal for achieving better roughness and lower cutting forces for the MDN431 material. Using Ti-coated tool, lesser cutting forces and tool better surface are observed which are due to the reduced coefficient of friction [36].

Table 8 Optimal process parameters for TiN/AlN-coated tool

Parameters	V_c	f	a_p	F_x	F_y	F_z	R_a
Desirability	59	0.062	0.25	65.44	95.05	122.31	0.66
MOPSO	59	0.062	0.28	60.57	95.68	121.99	0.68
Experimental	59	0.062	0.3	60.67	100.5	127.9	0.67

3.6 Confirmation Experiments

Mathematical models for the cutting forces and surface roughness are developed for the TiN/AlN multilayer coated tool using ANN and mathematical regression models. Regression models and trained ANN network are used to

predict the results for all the experimental conditions shown in Fig. 8 TiN/AlN multilayer coated tool.

Regression models are limited to predict the results within the boundary limits; hence, ANN models are developed to predict beyond the boundary limits. The coefficient of determination (R^2) represents the quality of the model. If it is closer to 1, the quality of the developed model is better. Regression models for TiN/AlN multilayer coated the cutting

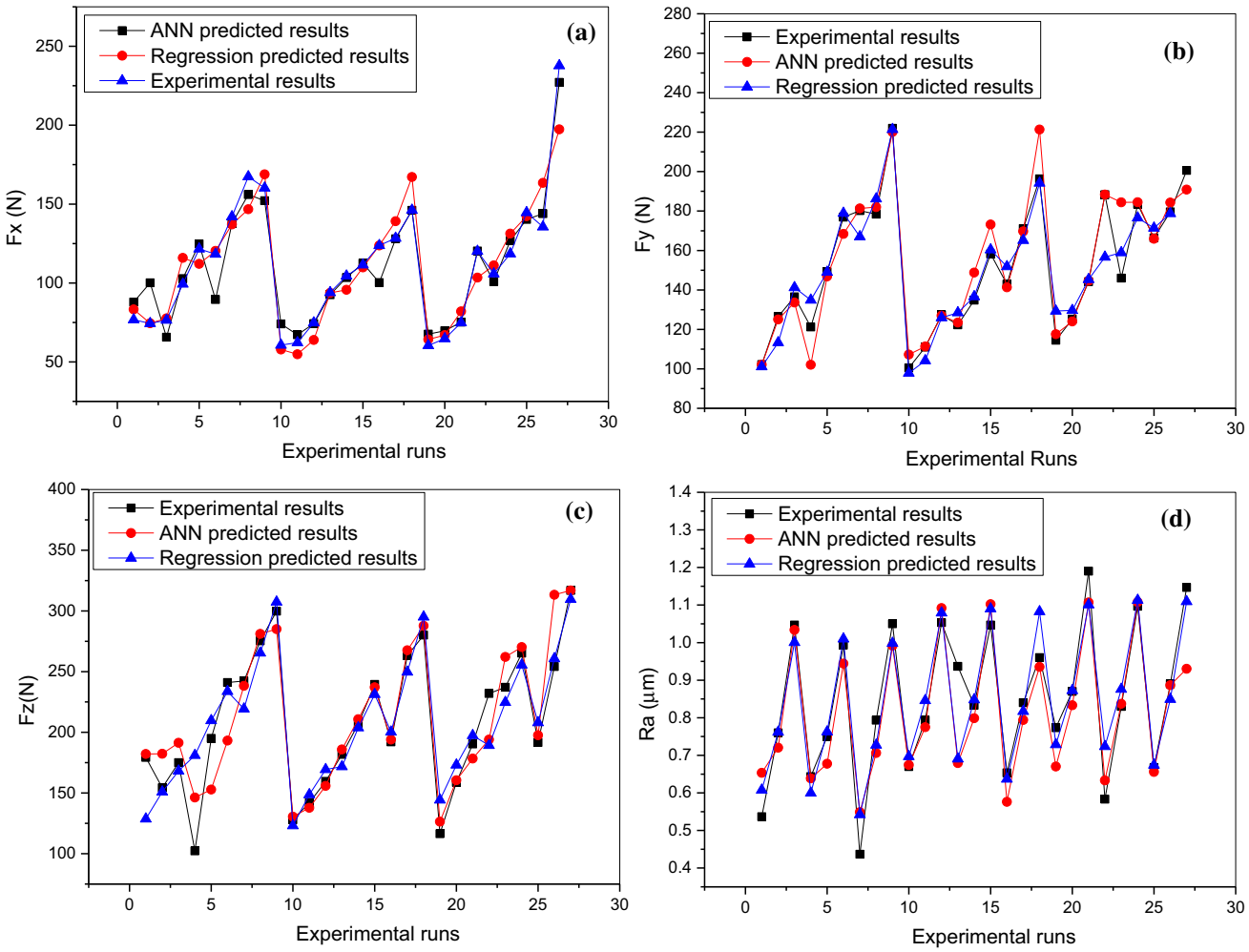

Fig. 8 Plots of experimental and predicted results

Table 9 Validation results for FTR-coated tool

Input			F_x			F_y			F_z			R_a		
a_p	V_c	f	Exp	Reg[a]	ANN[a]	Exp	Reg[a]	ANN[a]	Exp	Reg[a]	ANN[a]	Exp	Reg[a]	ANN[a]
0.2	59	0.062	75.29	83.26	76.59	101.20	101.10	101.93	125.50	128.68	113.20	0.56	0.61	0.55
0.25	75	0.07	99.50	99.48	93.58	118.65	128.82	115.64	178.99	181.40	144.06	0.70	0.69	0.96
0.35	118	0.078	136.56	137.02	98.14	150.65	160.79	125.34	226.57	227.82	210.10	0.85	0.74	0.88
0.2	59	0.087	78.98	75.29	77.55	120.65	109.82	116.55	159.50	147.01	160.67	0.70	0.73	0.71
0.25	118	0.093	140.56	138.96	108.75	175.55	171.33	177.32	255.65	254.20	269.52	0.88	0.78	0.99
0.35	75	0.1	100.56	102.15	91.10	146.56	146.64	156.44	218.86	217.76	231.44	0.90	0.91	0.92
0.2	59	0.117	76.56	75.67	70.15	138.56	132.81	141.17	166.56	164.42	153.32	0.93	0.93	0.97
0.25	118	0.125	168.55	164.03	164.81	223.50	203.41	219.66	295.56	297.86	273.60	1.00	1.05	0.91
0.35	75	0.078	120.76	95.65	119.71	141.25	139.09	140.66	194.65	195.25	199.44	0.75	0.78	0.70

[a]Predicted results

force and surface roughness (F_x, F_y, F_z and R_a) are obtained with R^2 values of 0.8902, 0.9161, 0.8342 and 0.8520 and absolute errors of 0.57, 0.34, 2.07 and 1.04%. Similarly, for ANN trained models for F_x, F_y, F_z and R_a are obtained with R^2 values are 0.9649, 0.9510, 0.9224 and 0.9094 and absolute errors of 1.17, 1.51, 2.12 and 2.59% (Fig. 8).

Plots of experimental and predicted results (Fig. 8) are found to be with least error and no significant deviation for the TiN/AlN multilayer coated tool. CoD (R^2) values of both the predictive models are close to 1, confirming the developed models are adequate. Validation of the developed models is represented in Table 9, and results are with negligible error [39]

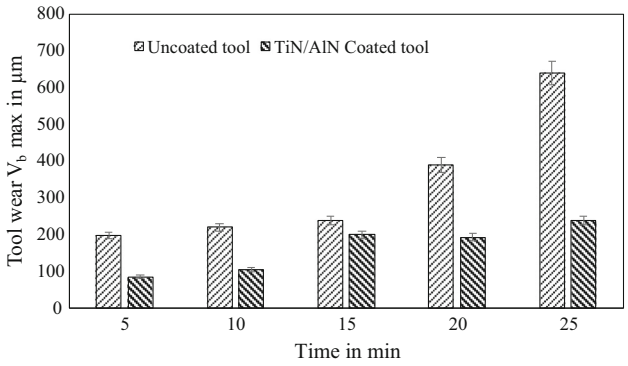

Fig. 9 Tool wear measurements for uncoated and coated tools

3.7 Tool Wear Measurements

Tool wear occurred during machining of the uncoated and coated tools at optimal process parameters studied with increments of time. Similar results are observed during studies of Inconel 718 in dry and cryogenic environments conducted by Musfira et al. [2].

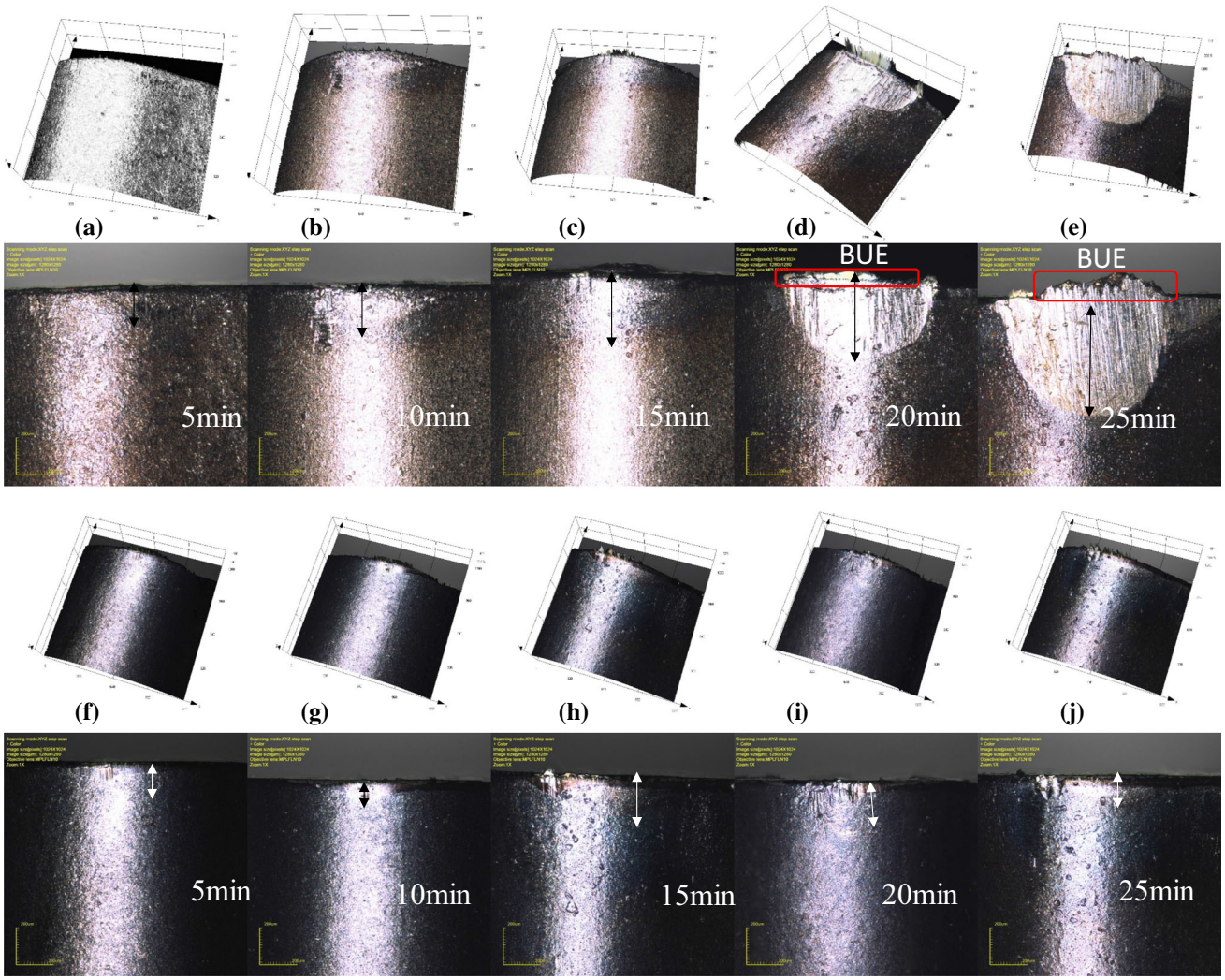

Fig. 10 Tool wear measurements for **a–e** uncoated tool and **f–j** coated tool

Figure 9 represents the tool wear analysis for uncoated and coated tools. According to the test results, the growth of tool wear under the uncoated tool is higher compared with the coated tool. Tool wear in TiN/AlN-coated tools is less compared with the uncoated tool. Figure 10 represents the tool wear measurements in coated and uncoated tools. Formation of built-up edge (BUE) was observed in the uncoated tool (Fig. 10d, e), and BUE is reduced in the coated tools. The abrasion wear mechanism was observed in both the coated and uncoated tools due to the presence of Cr and Ni phases in the MDN431 material [17]. Flank wear was observed in both the coated and uncoated tools. Tool wear was reduced by 105% in TiN/AlN-coated tool which is due to an increase in hardness of the coated tool and presence of nitrides of Ti and Al. AlN and TiN are hard phases of nitride which restricts the tool wear propagation. Flank wear propagation from the tool surface will be arrested by TiN layer; thereafter, AlN layer restricts which helps in increasing the tool life without affecting the performance. Due to an increase in elastic modulus on the coated surface, the stiffness in the coating is increased, which leads to an increase in deformation resistance. Tool wear which is being initiated from the top surface of the coatings is restricted by the hard phases with their high hardness and elastic modulus; though they deform elastically, it will regain its structure due to its modulus properties.

4 Conclusions

Experimental examination on the performance of TiN/AlN multilayer coated tools has been presented. The full factorial design was used for the analysis and validation of experiments.

- Multilayer thin-film coatings with the combination of TiN/AlN layers are successfully developed on WC–Co tool inserts. Coatings exhibit excellent adhesion quality characteristics with a coating thickness of 3.651 µm and HF1 adhesion quality observed for multilayer coatings.
- Mathematical regression models are developed for cutting forces and surface roughness using regression analysis and artificial neural network. CoD (R^2) of regression and ANN model is close to 1, confirming the developed model is adequate for TiN/AlN multilayer coated tool. Validation experiments indicate that the models presented can be further used for the selection, design and optimization of the machine tool, cutting tool in the process planning.
- Cutting force and surface roughness are optimized (minimization function) using MOPSO and desirability techniques and optimal process parameters are combination of $V_c = 59$ m/min, $f = 0.062$ mm/rev and $a_p = 0.28$ mm for TiN/AlN multilayer coated tool.
- Using TiN/AlN multilayer coated tools resulted in 9% reduction in surface roughness and cutting force. Tool wear has been reduced by 105% compared with the uncoated tool.

Acknowledgements The authors acknowledge the Department of Mechanical engineering NITK for all the encouragement and support. The authors acknowledge Mr. Gopinath. C. V, Head of Operations India, and Mr. K. Raveendra of R&D Department and QA Department Oerlikon Balzers Coating India Pvt., Ltd., Bangalore Plant, for providing all the testing facilities with encouragement and support.

References

1. Grzesik, W.; Niesłony, P.; Habrat, W.; Sieniawski, J.; Laskowski, P.: Investigation of tool wear in the turning of Inconel 718 superalloy in terms of process performance and productivity enhancement. Tribol. Int. **118**, 337–346 (2018). https://doi.org/10.1016/j.triboint.2017.10.005
2. Musfirah, A.H.; Ghani, J.A.; Haron, C.H.C.: Tool wear and surface integrity of Inconel 718 in dry and cryogenic coolant at high cutting speed. Wear **376–377**, 125–133 (2017). https://doi.org/10.1016/j.wear.2017.01.031
3. Chabbi, A.; Yallese, M.A.; Meddour, I.; Nouioua, M.; Mabrouki, T.; Girardin, F.: Predictive modeling and multi-response optimization of technological parameters in turning of Polyoxymethylene polymer (POM C) using RSM and desirability function. Meas. J. Int. Meas. Confed. **95**, 99–115 (2017). https://doi.org/10.1016/j.measurement.2016.09.043
4. Hanief, M.; Wani, M.F.; Charoo, M.S.: Modeling and prediction of cutting forces during the turning of red brass (C23000) using ANN and regression analysis. Eng. Sci. Technol. Int. J. **20**, 1220–1226 (2017). https://doi.org/10.1016/j.jestch.2016.10.019
5. Mia, M.; Dhar, N.R.: Response surface and neural network based predictive models of cutting temperature in hard turning. J. Adv. Res. **7**, 1035–1044 (2016). https://doi.org/10.1016/j.jare.2016.05.004
6. Das, S.R.; Dhupal, D.; Kumar, A.: Experimental investigation into machinability of hardened AISI 4140 steel using TiN coated ceramic tool. Meas. J. Int. Meas. Confed. **62**, 108–126 (2015). https://doi.org/10.1016/j.measurement.2014.11.008
7. Zhang, S.; Wu, W.; Chen, W.; Yang, S.: Structural optimisation and synthesis of multilayers and nanocomposite AlCrTiSiN coatings for excellent machinability. Surf. Coatings Technol. **277**, 23–29 (2015). https://doi.org/10.1016/j.surfcoat.2015.07.033
8. Kumar, R.; Chauhan, S.: Study on surface roughness measurement for turning of Al 7075/10/SiCp and Al 7075 hybrid composites by using response surface methodology (RSM) and artificial neural networking (ANN). Meas. J. Int. Meas. Confed. **65**, 166–180 (2015). https://doi.org/10.1016/j.measurement.2015.01.003
9. Suresh, R.; Basavarajappa, S.; Gaitonde, V.N.: Experimental studies on the performance of multilayer coated carbide tool in hard turning of high strength low alloy steel. J. Mater. Res. **30**, 3056–3064 (2015). https://doi.org/10.1557/jmr.2015.236
10. Bhat, D.G.: A review of: "Handbook of physical vapor deposition (PVD) processing film formation, adhesion, surface preparation and contamination control". Mater. Manuf. Processes **14**, 783 (1999)
11. Kivak, T.: Optimization of surface roughness and flank wear using the Taguchi method in milling of Hadfield steel with PVD and CVD coated inserts. Meas. J. Int. Meas. Confed. **50**, 19–28 (2014). https://doi.org/10.1016/j.measurement.2013.12.017

12. Arulkirubakaran, D.; Senthilkumar, V.: Performance of TiN and TiAlN coated micro-grooved tools during machining of Ti–6Al–4V alloy. Int. J. Refract. Met. Hard Mater. **62**, 47–57 (2017). https://doi.org/10.1016/j.ijrmhm.2016.10.014
13. Noordin, M.Y.; Venkatesh, V.C.; Chan, C.L.; Abdullah, A.: Performance evaluation of cemented carbide tools in turning AISI 1010 steel. J. Mater. Process. Technol. **116**, 16–21 (2001). https://doi.org/10.1016/S0924-0136(01)00838-X
14. Qin, F.; Hu, J.; Chou, Y.K.; Thompson, R.G.: Delamination wear of nano-diamond coated cutting tools in composite machining. Wear. **267**, 991–995 (2009). https://doi.org/10.1016/j.wear.2008.12.065
15. Sahoo, A.K.; Sahoo, B.: A comparative study on performance of multilayer coated and uncoated carbide inserts when turning AISI D2 steel under dry environment. Meas. J. Int. Meas. Confed. **46**, 2695–2704 (2013). https://doi.org/10.1016/j.measurement.2013.04.024
16. Sahoo, A.K.; Sahoo, B.: Experimental investigations on machinability aspects in finish hard turning of AISI 4340 steel using uncoated and multilayer coated carbide inserts. Meas. J. Int. Meas. Confed. **45**, 2153–2165 (2012). https://doi.org/10.1016/j.measurement.2012.05.015
17. Coelho, R.T.; Ng, E.G.; Elbestawi, M.A.: Tool wear when turning hardened AISI 4340 with coated PCBN tools using finishing cutting conditions. Int. J. Mach. Tools Manuf. **47**, 263–272 (2007). https://doi.org/10.1016/j.ijmachtools.2006.03.020
18. Scheerer, H.; Hoche, H.; Broszeit, E.; Schramm, B.; Abele, E.; Berger, C.: Effects of the chromium to aluminum content on the tribology in dry machining using (Cr, Al)N coated tools. Surf. Coatings Technol. **200**, 203–207 (2005). https://doi.org/10.1016/j.surfcoat.2005.02.112
19. Prabhu, S.; Vinayagam, B.K.: Analysis of surface characteristics by electrolytic in-process dressing (ELID) technique for grinding process using single wall carbon nano tube-based nanofluids. Arab. J. Sci. Eng. **38**, 1169–1178 (2013). https://doi.org/10.1007/s13369-012-0355-6
20. Bhalamurugan, R.; Prabhu, S.: Performance characteristic analysis of automated robot spray painting using Taguchi method and gray relational analysis. Arab. J. Sci. Eng. **40**, 1657–1667 (2015). https://doi.org/10.1007/s13369-015-1628-7
21. Shihab, S.K.: Optimization of WEDM process parameters for machining of friction-stir-welded 5754 aluminum alloy using Box–Behnken design of RSM. Arab. J. Sci. Eng. **43**, 5017–5027 (2018). https://doi.org/10.1007/s13369-018-3238-7
22. Prabhu, S.; Vinayagam, B.K.: AFM nano analysis of Inconel 825 with single wall carbon nano tube in die sinking EDM process using Taguchi analysis. Arab. J. Sci. Eng. **38**, 1599–1613 (2013). https://doi.org/10.1007/s13369-012-0348-5
23. Vasu, M.; Nayaka, H.S.: Investigation of cutting force tool tip temperature and surface roughness during dry machining of spring steel. Mater. Today Proc. **5**, 7141–7149 (2018). https://doi.org/10.1016/j.matpr.2017.11.379
24. Malghan, R.L.; Rao, K.M.C.; Shettigar, A.K.; Rao, S.S.; D'Souza, R.J.: Application of particle swarm optimization and response surface methodology for machining parameters optimization of aluminium matrix composites in milling operation. J. Braz. Soc. Mech. Sci. Eng. **39**, 3541–3553 (2017). https://doi.org/10.1007/s40430-016-0675-7
25. Nayak, M.; Sehgal, R.: Effect of tool material properties and cutting conditions on machinability of AISI D6 steel during hard turning. Arab. J. Sci. Eng. **40**, 1151–1164 (2015). https://doi.org/10.1007/s13369-015-1578-0
26. Ashrith, H.S.; Doddamani, M.; Gaitonde, V.; Gupta, N.: Hole quality assessment in drilling of glass microballoon/epoxy syntactic foams. JOM **70**, 1–6 (2018). https://doi.org/10.1007/s11837-018-2925-x
27. Vasu, M.; Nayaka, H.S.: Investigation of machinability characteristics on EN47 steel for cutting force and tool wear using optimization technique. Mater. Res. Express (2018). https://doi.org/10.1088/2053-1591/aac67f
28. Ravindran, P.; Manisekar, K.; Narayanasamy, P.; Selvakumar, N.; Narayanasamy, R.: Application of factorial techniques to study the wear of Al hybrid composites with graphite addition. Mater. Des. **39**, 42–54 (2012). https://doi.org/10.1016/j.matdes.2012.02.013
29. Selvakumar, N.; Narayanasamy, P.: Optimization and effect of weight fraction of MoS_2on the tribological behavior of Mg–TiC–MoS_2 hybrid composites. Tribol. Trans. **59**, 733–747 (2016). https://doi.org/10.1080/10402004.2015.1110866
30. Narayanasamy, P.; Selvakumar, N.: Effect of hybridizing and optimization of TiC on the tribological behavior of Mg–MoS_2 composites. J. Tribol. **139**, 051301 (2017). https://doi.org/10.1115/1.4035383
31. Ravindran, P.; Manisekar, K.; Narayanasamy, R.; Narayanasamy, P.: Tribological behaviour of powder metallurgy-processed aluminium hybrid composites with the addition of graphite solid lubricant. Ceram. Int. **39**, 1169–1182 (2013). https://doi.org/10.1016/j.ceramint.2012.07.041
32. Aslantas, K.; Ucun, T.I.; Çicek, A.: Tool life and wear mechanism of coated and uncoated Al_2O_3/TiCN mixed ceramic tools in turning hardened alloy steel. Wear **274–275**, 442–451 (2012). https://doi.org/10.1016/j.wear.2011.11.010
33. Ciurana, J.; Arias, G.; Ozel, T.: Neural network modeling and particle swarm optimization (PSO) of process parameters in pulsed laser micromachining of hardened AISI H13 steel. Mater. Manuf. Processes **24**, 358–368 (2009). https://doi.org/10.1080/10426910802679568
34. Kumar, B.R.; Vardhan, H.; Govindaraj, M.; Saraswathi, S.P.: Artificial neural network model for prediction of rock properties from sound level produced during drilling. Geomech. Geoeng. **8**, 53–61 (2013). https://doi.org/10.1080/17486025.2012.661469
35. Vidakis, N.; Antoniadis, A.; Bilalis, N.: The VDI 3198 indentation test evaluation of a reliable qualitative control for layered compounds. J. Mater. Process. Technol. **143–144**, 481–485 (2003). https://doi.org/10.1016/S0924-0136(03)00300-5
36. Badiger, P.V.; Desai, V.; Ramesh, M.R.: Development and characterization of Ti/TiC/TiN coatings by cathodic arc evaporation technique. Trans. Indian Inst. Met. **70**, 2459–2464 (2017). https://doi.org/10.1007/s12666-017-1107-9
37. Lawal, J.; Kiryukhantsev-Korneev, P.; Matthews, A.; Leyland, A.: Mechanical properties and abrasive wear behaviour of Al-based PVD amorphous/nanostructured coatings. Surf. Coatings Technol. **310**, 59–69 (2017). https://doi.org/10.1016/j.surfcoat.2016.12.031
38. Bouacha, K.; Yallese, M.A.; Mabrouki, T.; Rigal, J.F.: Statistical analysis of surface roughness and cutting forces using response surface methodology in hard turning of AISI 52100 bearing steel with CBN tool. Int. J. Refract. Met. Hard Mater. **28**, 349–361 (2010). https://doi.org/10.1016/j.ijrmhm.2009.11.011
39. Angadi, S.B.; Melinamani, R.; Gaitonde, V.N.; Doddamani, M.; Karnik, S.R.: Experimental investigations on drilling characteristics of cenosphere reinforced epoxy composites. Appl. Mech. Mater. **766–767**, 801–811 (2015). https://doi.org/10.4028/www.scientific.net/AMM.766-767.801
40. Sukumar, M.S.; Venkata Ramaiah, P.; Nagarjuna, A.: Optimization and prediction of parameters in face milling of Al-6061 using Taguchi and ANN approach. Proc. Eng. **97**, 365–371 (2014). https://doi.org/10.1016/j.proeng.2014.12.260